REPORT DOCUMENTATION PAGE

Form Approved
OMB No. 0704-0188

1. REPORT DATE *(DD-MM-YYYY)*	2. REPORT TYPE	3. DATES COVERED *(From - To)*
22/05/2019	Final Technical	1/1/2014 to 8/1/2017

4. TITLE AND SUBTITLE

High-Power-Density High-Efficiency Carbon Nanotube Thermo-Acoustic (TA) Projectors

5a. CONTRACT NUMBER

5b. GRANT NUMBER

N00014-14-1-0158

5c. PROGRAM ELEMENT NUMBER

6. AUTHOR(S)

Prashant Kumar, Yongke Yan and Shashank Priya

5d. PROJECT NUMBER

5e. TASK NUMBER

5f. WORK UNIT NUMBER

7. PERFORMING ORGANIZATION NAME(S) AND ADDRESS(ES)

Center for Energy Harvesting Materials and Systems,
Virginia Tech, Blacksburg, VA 24061

8. PERFORMING ORGANIZATION REPORT NUMBER

9. SPONSORING/MONITORING AGENCY NAME(S) AND ADDRESS(ES)

Office of Naval Research
875 North Randolph Street
Arlington, VA 22203-1995

10. SPONSOR/MONITOR'S ACRONYM(S)

ONR

11. SPONSOR/MONITOR'S REPORT NUMBER(S)

12. DISTRIBUTION/AVAILABILITY STATEMENT

No restrictions

13. SUPPLEMENTARY NOTES

- Fabrication of high power projector (for low frequency) sheets and reliable encapsulation for more efficient performance.
- Develeoped the complete model of thermo-vibro-acoutic- fluid structure intercation to understand the device performance in different fluids/gases.
- Demonstrated the practicality of TA device for relatively lower range of frequency band.

14. ABSTRACT

Here we provide detailed model involving structure-fluid-acoustic interaction explaining the physical behavior of Thermoacoustic projectors (TAPs). Numerical model combines all the controlling steps from power input to acoustic wave generation to the propagation in outer fluid media. Power input to the computational domain is used to determine the frequency dependent temperature variation and thermal diffusive length which governs the generation of TA wave. TA wave is used as driving force to simulate the vibration of the structure and produce acoustic wave in outer fluids (air or water). A high power LF device (<180 Hz) is fabricated to validate the model and demonstrate the low frequency projector. The detailed experimental analysis (vibration and acoustics) are performed on the fabricated devices in both air and water medium and results are compared with the predictions from modeling.

15. SUBJECT TERMS

16. SECURITY CLASSIFICATION OF:			17. LIMITATION OF ABSTRACT	18. NUMBER OF PAGES	19a. NAME OF RESPONSIBLE PERSON
a. REPORT	b. ABSTRACT	c. THIS PAGE			Dr. Yongke Yan
U	U	U	UU	15	19b. TELEPHONE NUMBER *(Include area code)*

High-Power-Density High-Efficiency Carbon Nanotube Thermo-Acoustic (TA) Projectors

Prashant Kumar, Yongke Yan and Shashank Priya
Center for Energy Harvesting Materials and Systems, Virginia Tech, Blacksburg, VA 24061
Award Number: N00014-14-1-0158
http://www.me.vt.edu/cehms/

LONG-TERM GOALS

Realize the high acoustical power output in wide-band thermoacoustic (TA) projector (encapsulated between two thin, lightweight and flexible membranes) and narrow-band low frequency resonant TA projector (encapsulated between two plates with high flexural rigidity).

OBJECTIVES

- Fabrication of high power projector (for low frequency) sheets and reliable encapsulation for more efficient performance.
- Characterize the TA device to find the acoustic behavior in air medium.
- Characterize the TA device to evaluate the performance under different water loading.
- Develeoped the complete model of thermo-vibro-acoutic- fluid structure intercation to understand the device performance in different fluids/gases.

APPROACH

This is a collaborative project between three institutions. Brief summary of tasks for each institution is listed below.

University of Texas – Dallas

- Optimization of proejctor performance by using carbon nanotube sheet and yarns with different characteristics. The prototypical projectors sheets investigated will contain ~10 nm diameter MWNTs that are ~400 μm long.
- Construction and evaluation of various sonar projectors geometries, including those in which nanotube projector sheets are either free standing single layer, orthogonaly superimposed multilayered structure or spatially separated tandem arrays. Both encapsulated resonant and wide-band projectors will be constructed and evaluated.
- Studies will be conducted on: various transmission medias, CNT sheet types, array geometries of CNT prjector sheets.
- Fabrication of projector sheets that provide more unifrom current transport.
- Fabrication of TA projectors with different compliance properties.

Virginia Tech

- Device characterization
  - Mechanical characterization.
  - Acoustic characterization.
  - Thermal characterization.
  - Fluid-Structure interraction in water medium.
- Evaluation of thermally conductive coatings.
- Mechanical/vibrational modeling of encapsulated TA projectors.
- Coupled model that can take electrical input and provide sound as the output [mechanical – thermal and acoustic layers]

NUWCDIVNPT

- Physics-based modeling of thermoacoustic transduction.
- Acoustic performance testing.

WORK COMPLETED

- Demonstrated the practicality of TA device for relatively lower range of frequency band.
- Vibrational characterization of TA device in both air and water medium.
- Underwater acoustic experimental setup and characterization
- Conceptualization of more inclusive and mutilayer modeling of the TA device.
- Vibro-Acoutic Finte Element modeling is developed and solved for the dvice

Results:

Modeling of TA Device

The unique feature of this device is the synchronization of various physics for single output that is acoustic pressure. Figure 1 provides the schematic of multilayer model that includes physics of the device as follows:

- ❑ 1st Layer
  - Primary purpose is to quantify the energy dissipation from the MWCNT sheet and evaluate its impact on generation of the pressure wave.
  - Develop the understanding of TA wave generation with different gaseous mediums and validate the experimental results.
  - Analyze spatial distribution of pressure and input for the other layers
- ❑ 2nd Layer:
  - Develop the understanding of vibration characteristic of device in air and water medium and evaluate its effect on incident of TA pressure wave.
- ❑ 3rd Layer:
  - Quantify the impact of vibration on sound generation in surrounding (air and water)

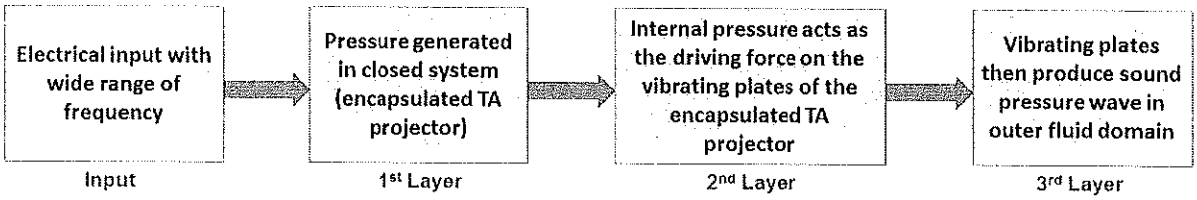

Figure 1: Multilayer model layout for TA projectors.

Layer 1: Thermoacoustic modeling

Several researchers have developed the experimental and analytical model of heat transfer from CNT in the surrounding media and subsequently TA generation. But only few have illustrated the enclosed boundary conditions similar to our device [1-5]. Hu et al. [6] studied the decay of thermal wavelength with respect to thermal diffusion length but it seems the system resonance condition (effect of reflected waves) was not addressed. The goal of this modeling exercise is to investigate the TA generation and heat transfer analysis from CNTs for the encapsulated device to enhance the efficiency. According to Lim et al. [3] and considering the fact that MWCNTs do not retain significant heat, all the sinusoidal input current, I, for CNT resistance R at frequency $\omega/2$ (heating twice each periodic cycle) (Eq. 1) would be converted into thermal power (P_{in}). This demonstrates that, in TA transducers, the sinusoidal power will be used to heat the surrounding on a temporal basis and generate the TA waves. The near field TA pressure waves will then act as the driving force for the vibration of the encapsulated plates which has been incorporated in vibro-acoustic modeling block.

$$\left(I \sin\frac{1}{2}\omega t\right)^2 R = P_{in} - P_{in}e^{i\omega t} \tag{1}$$

Considering the near field TA wave as planar wave, the general form of time dependent equations[3] showing thermo-acoustic coupling are given by Eq.2 and 3:

$$\frac{\partial^2 p}{\partial t^2} - \frac{P_0}{\rho_0}\frac{\partial^2 p}{\partial x^2} = \frac{P_0}{T_0}\frac{\partial^2 T}{\partial t^2} \tag{2}$$

$$\frac{\partial T}{\partial t} - \alpha\frac{\partial^2 T}{\partial x^2} = \frac{\gamma - 1}{\gamma}\frac{T_0}{P_0}\frac{\partial p}{\partial t} \tag{3}$$

where ρ_0 = gas density, α =thermal diffusivity, $\gamma = C_p / C_v$(heat capacity ratio of gas), T_0 and P_0 ambient temperature and pressure. Reference 6 also shows the comprehensive heat equations considering all the possible factors along with instantaneous heat exchange given as:

$$P_{in} - P_{in}e^{i\omega t} = a\beta T_{su} + aQ_0 + \frac{a}{2}c\frac{d(T_{su})}{d} \tag{4}$$

Where a = total thin film area of CNT, β= per unit area heat loss, Q_0= instantaneous heat transfer to surrounding, c = per area heat capacity and T_{su}=surrounding temperature difference. The equations included here will provide the base for understanding the mechanism of TA generation in closed and encapsulated environment.

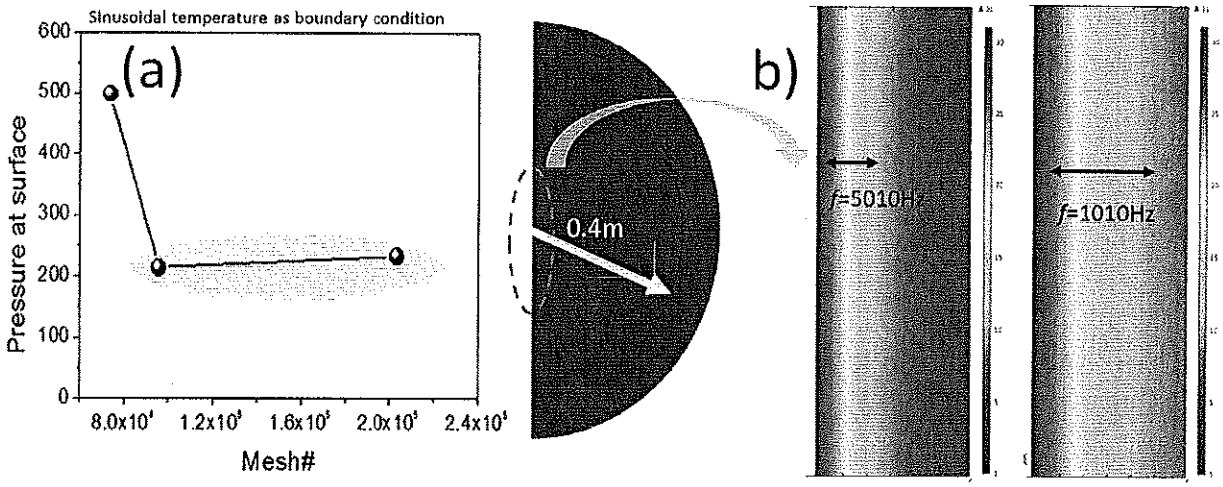

Figure 2: (a) Mesh sensitivity test results, (b) Thermal diffusion length at two different frequencies.

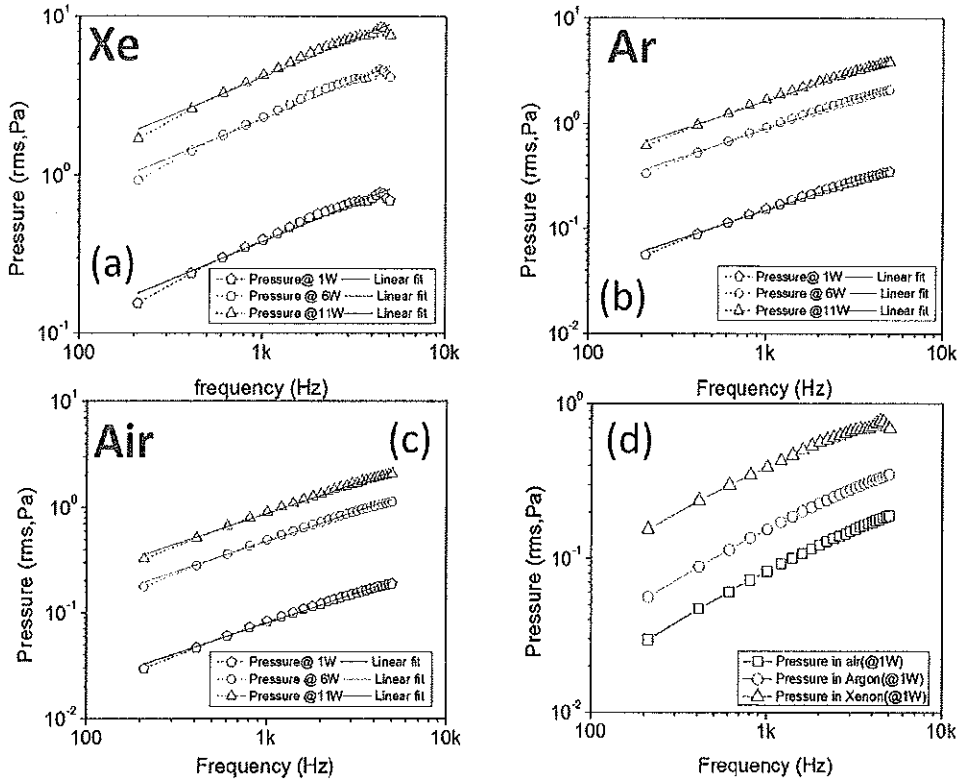

Figure 3: (a) TA pressure at r = 2cm in surrounding medium (open) at different frequencies, a pressure in Xenon, (b) TA pressure in Argon, (c) TA pressure in Air, (d) Comparison of pressure with different surrounding gases.

We have developed a comprehensive FEM model (along with required governing equations) for current transducers which covers the phenomenon proposed in above modeling block diagram (Figure 1). Starting with the thermal power input (evaluated from joule heating, I^2R) a detailed study is being developed for the thermoacoustic generation from sinusoidal heat source in nearby fluidic environment. COMSOL v4.3 is being used for numerical calculations. Before starting any computational study we check the mesh sensitivity of our model to avoid the loss in accuracy at the cost of high computational cost. Figure 2 (a) shows that 2nd mesh is better for our numerical analysis. We understand that the most of the volume of CNT sheet is occupied by nearby fluid, and it's extremely difficult to model a real CNT sheet in FEM (thus necessitating the development of molecular dynamics model), therefore, we assume the very thin layer of nearby surrounding medium (like Air, Argon and Xenon) of approximately 18 micron thickness as heat source for thermal wave generation. The fluid domain length for this 1st layer of modeling is shown in Figure 2(b). The spherical nearby fluid medium is chosen for thermoacoustic wave traveling along with a 0.1m of perfectly matched layer (PML). PML played a key role in our modeling by avoiding any back reflection in acoustic domain. This helped us in evaluating the accurate pressure field around

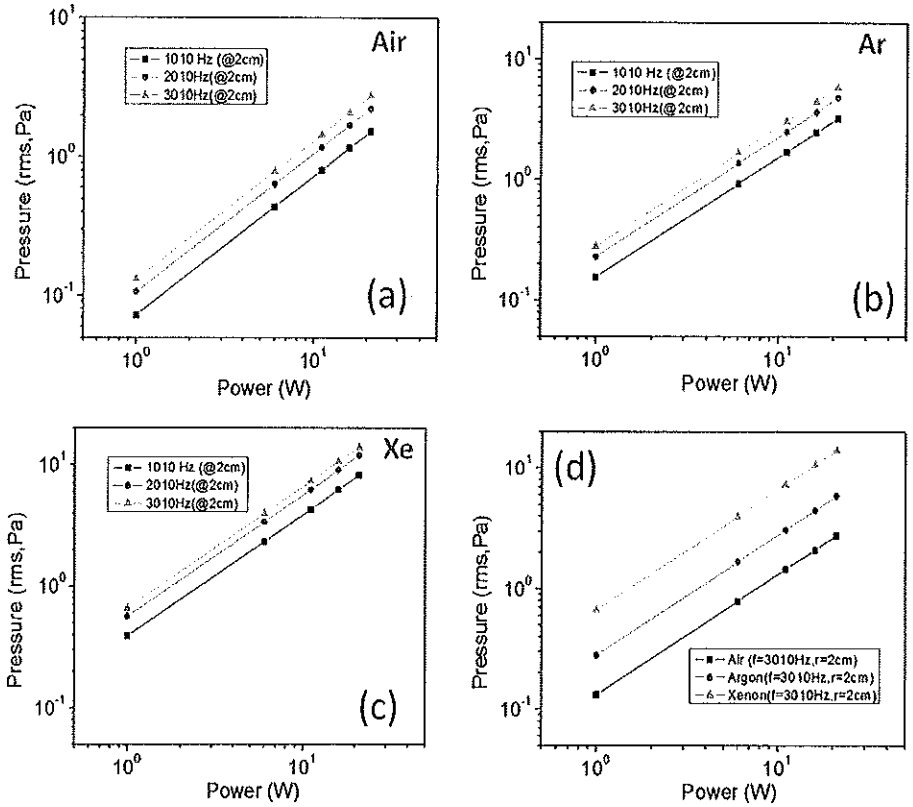

Figure 4: (a) TA pressure in surrounding medium (open) at different input thermal power, (b) TA pressure in Argon, (c) TA pressure in Xenon, (d) Comparison of pressure with different surrounding gases.

the device with no reflective or scattered pressure wave. Figure 2 (b) shows the quantitative depiction of thermal wave length during TA generation. It is evident from the images that with

increase of frequency, thermal diffusive length decreases ($l = \sqrt{\alpha / \pi f}$, α - thermal diffusivity, and f - heating frequency). The thermal diffusion length represents the heat distribution from the heat source at a particular frequency in nearby space and determines the generation of TA wave. We have evaluated the diffusion length for three different mediums: Xenon (Xe), Argon (Ar) and air. From our modeling the lengths are: Xe = ~27μm, Ar= ~45μm and Air= ~47.4 μm at 3010Hz. This analysis will be further extended to higher molecular density gases

A detailed thermoacoustic frequency analysis is being conducted with different parameters such as power input and surrounding medium. The frequency response up to 10 kHz has been obtained in our ongoing numerical study. Figure 3 (in log-scale) shows the comparative study of TA pressure generated with different aforementioned parameters, which predicts the experimentally verified linear trend of acoustic pressure versus frequency. Figure 3(d) provides the comparative study in the frequency domain for different surrounding gases. In addition, we also compared the pressure generated at various powers for a fixed frequency, which is shown in Figure 4 for three gases. All the numerically solved pressure values are recorded at a point 2cm above the CNT sheet. This 1st layer of study is important because the output from this model will be directly considered as input for the 2nd layer of modeling mentioned above.

Experimental:

Next, acoustic measurements were conducted at 2nd peak frequency (performance is dominant) for different range of parameters. Figure 5(a) shows the acoustic pressure at 3 cm of the device at different average power input. The device shows the linear trend. To avoid excessive heating of the device we used a large aluminum plate as the bottom plate (for heat dissipation) and limited our experiments at the low power. Figure 5(b) shows the acoustic pressure with variable distance. Pressure in the near field (approximately up to Raleigh distance: Area/Wavelength) was random, but on increasing the distance it followed the decreasing trend approximately 6 dB on doubling the distance. It is also observed from the experiments that on scanning the acoustic output at different points across the diagonal (Figure 5(c)), pressure first increased and then decreased. It shows the symmetry with respect to the central line which is similar to the mode shape obtained. All the experiments in air medium successfully demonstrates the low frequency operation (580 and 972 Hz) of the fabricated device. Figure 5(d) compares the performance of open sheet (theoretical) and encapsulated device. A large gain in acoustic pressure (Q factor higher) clearly shows the merits of encapsulation over open device for low frequency applications.

After characterizing the device in the air medium, experiments were setup for the underwater testing. A detailed experimental setups were developed in water tank to understand the acoustic behavior of the device and the impact of water loading on vibration. Figure 6 show the water tank experimental setup. Scanning head vibrometer (Polytec PDV-500) were used to measure the vibration. The transducer was mounted on vertical rod-plate structure and hydrophone was placed

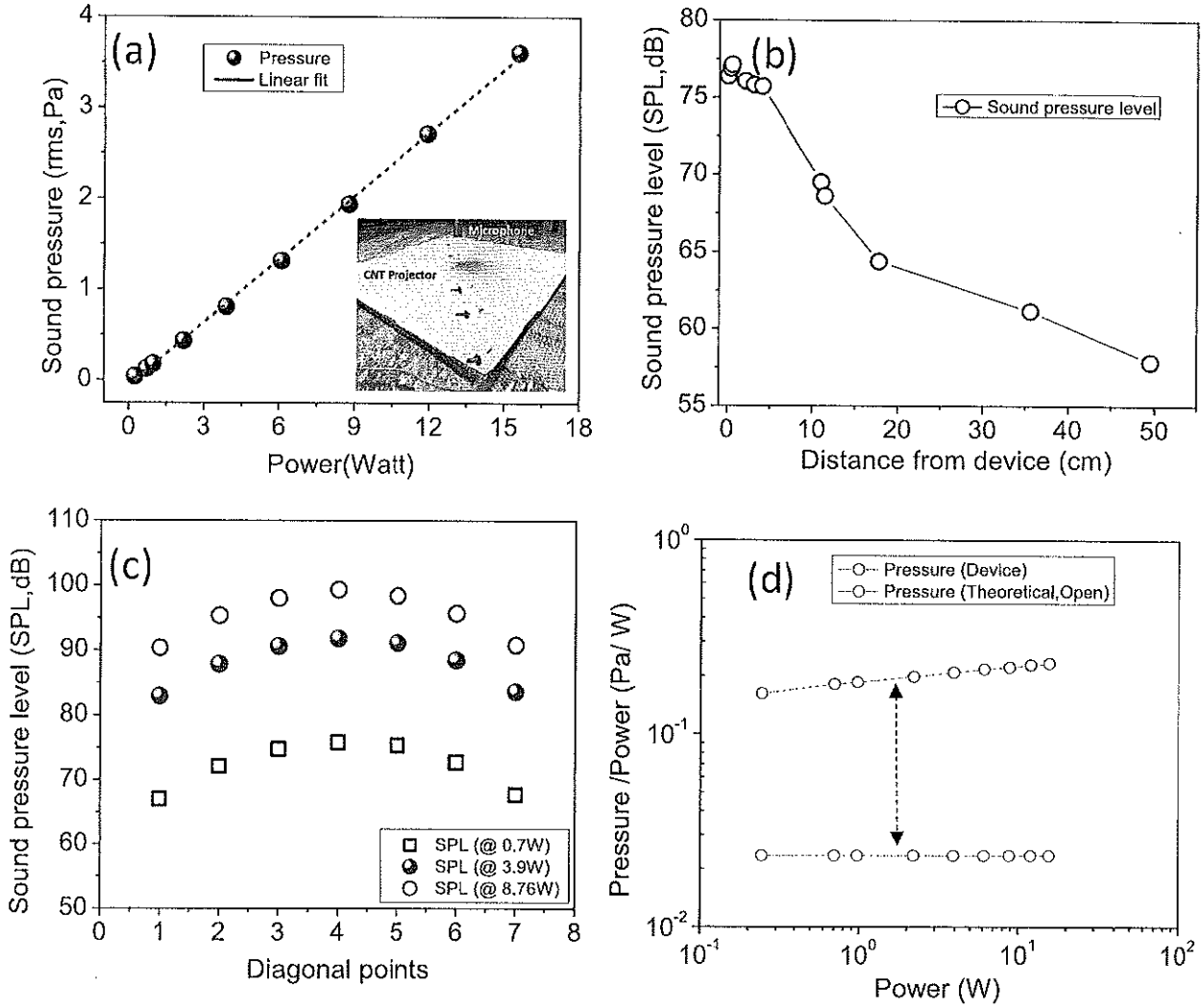

Figure 5: (a) Linear trend of SPL in air with input power to the device, (b) Sound pressure level (SPL) in air with increase of distance from the device, (c) Sound pressure level (SPL) across the diagonal point at different input power, (d) Comparison of acoustic performance of device with open system (theoretical)

3 cm (Brüel & Kjær 8103) away from the transducer. The rod was fixed at top and bottom to avoid any pendulum effect during device vibration. Figure 7 (a) and (b) show the acoustic and vibrational frequency response of the transducer under different water loading (at 0, 1 and 2 feet water depth) on applying the burst chirp signal input for wide frequency range (0-2000Hz). Power input was maintained constant while recording the vibrational response. These results show that in water medium only the first mode is dominant. Figure 7 (c) shows the correlation between the height of water loading and resultant change in frequency of the system. As it can be seen from the results, first the frequency decreased from zero water loading to one feet of water loading and then increased from first feet to second feet of water loading. This behavior can be explained by accounting the effect of entrained gas between the encapsulated device and the non-linear behavior of elastomer support at the edges under different hydrostatic pressure.

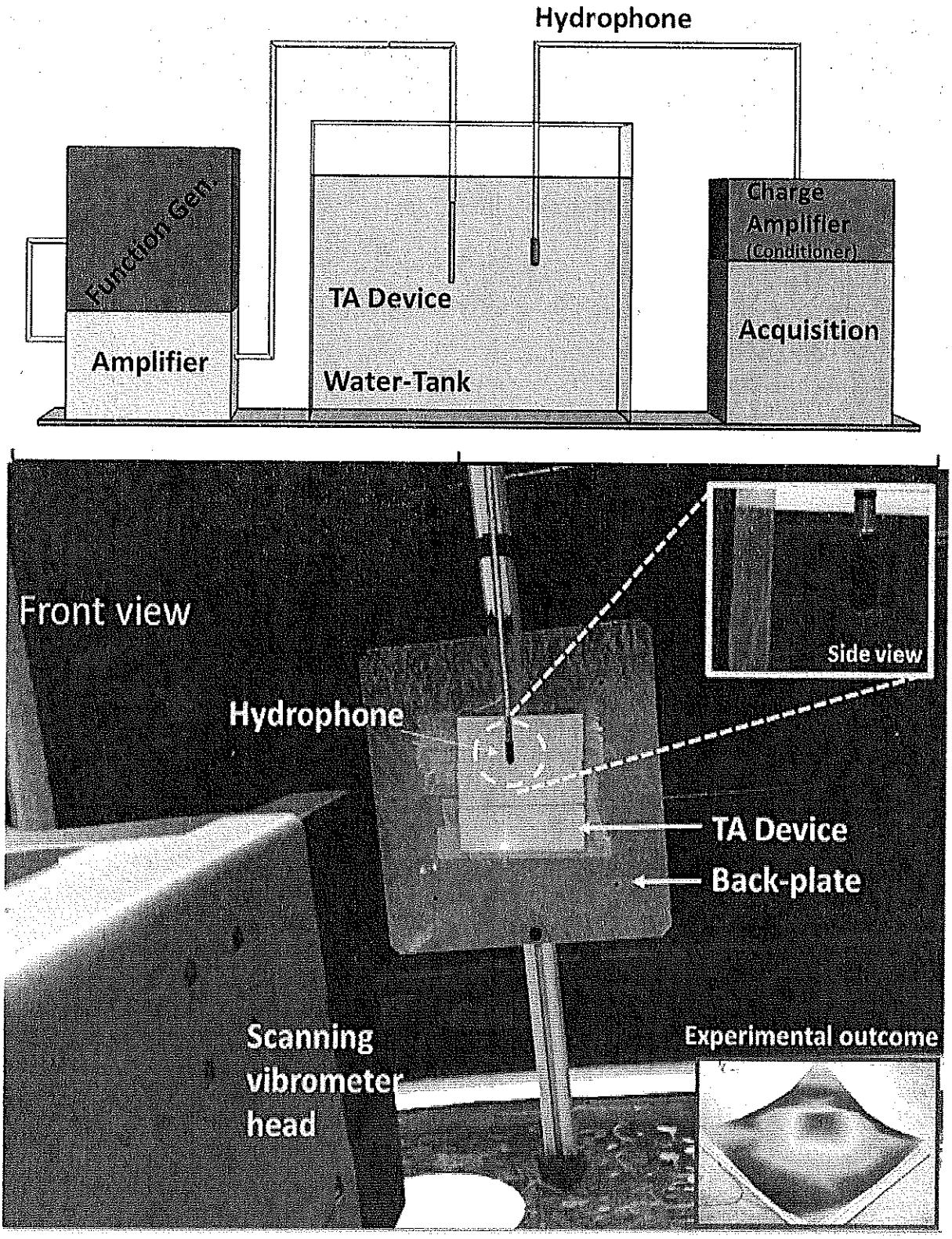

Figure 6: Schematics and experimental setup for acoustic and vibration measurement in large tank

Figure 7 (d) shows the results for output pressure as a function of input power. Generated pressure followed the linear path with lower input power and became non-linear at higher power. The saturation limit occurs because the number of argon molecules in transducer are constant so they cannot provide increasing linear acoustic pressure with increasing input power after a threshold. Also, bigger tank provides relatively less reflection than smaller tank. These underwater experiments demonstrate the ultra-low frequency nature of fabricated projector.

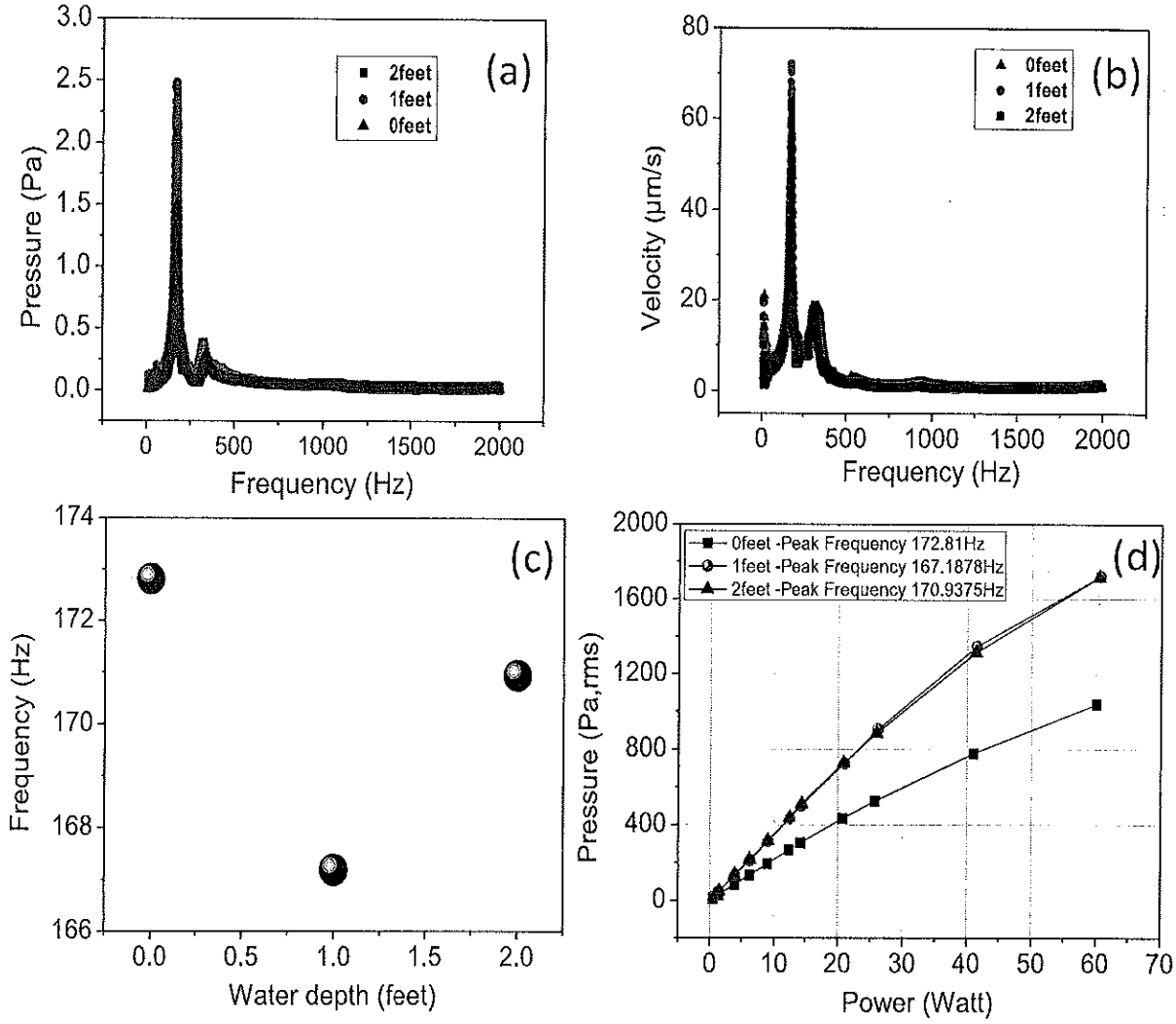

Figure 7: (a) Velocity frequency response of the device under different water loading (burst chirp input), (b) Pressure frequency response for different water loading, (c) water loading vs frequency variation and, (d) pressure with different power at different loading (with sinusoidal input)

Layers 2&3: Vibro-acoustic modeling

In 1st layer, we focused on the thermoacoustic wave motion in "open" fluid domain. However, dynamics will change if the TA generating heat source becomes confined inside a resonating structure. In these steps, we compute the coupled behavior of the inner fluid / vibrating structure and vibration structure / outer fluid, respectively. The structural dynamics and TA wave interact to produce the acoustic wave outside the encapsulated device called a vibro-acoustic wave. Figure 8 shows the schematic for vibro-acoustic modeling which represents the normal incidence of the TA wave on the plate and spherical sound wave generation in the outer medium. We have made some assumptions in this analysis:

- Due to the small gap between the CNT sheet and encapsulating plates, the incident TA wave is considered a plane wave (already evaluated by integrated model)
- The transmission and transmission loss through the aluminum plate is considered negligible, since there is a huge impedance mismatch between Argon and the plate

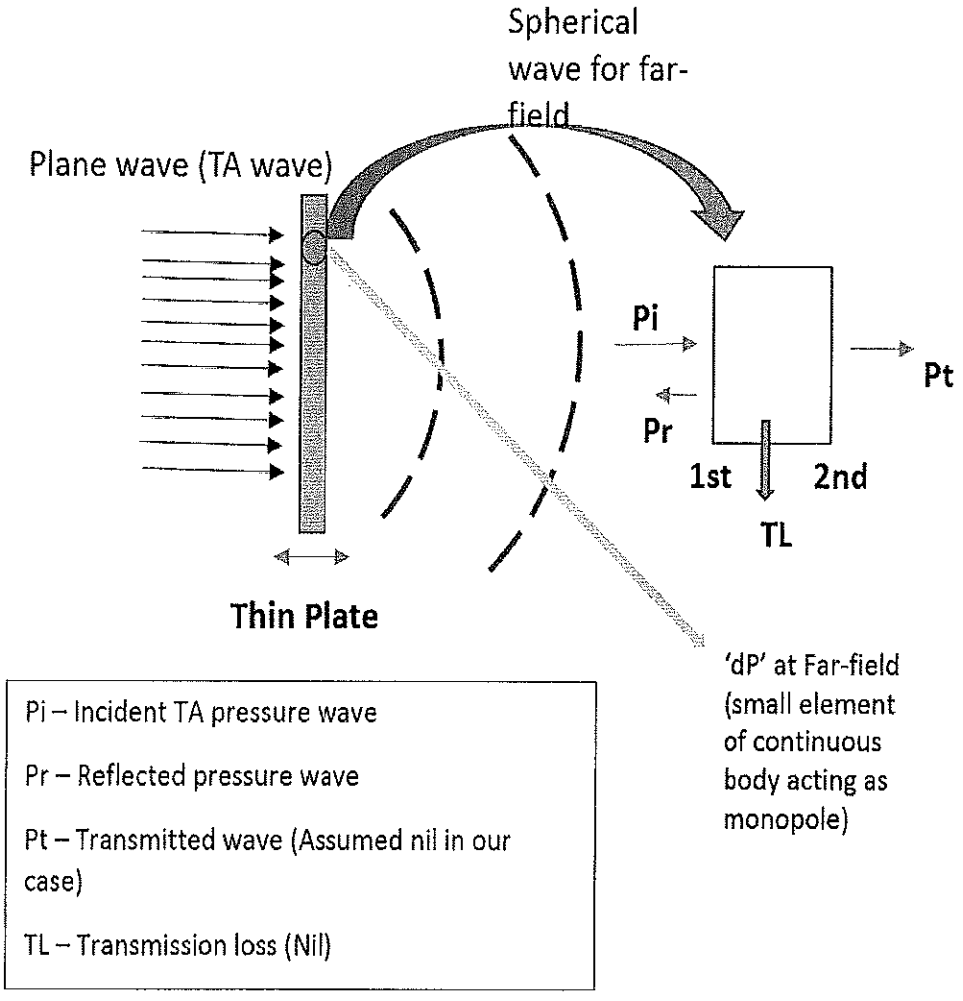

Figure 8: Schematic showing vibro-acoustic layer of modeling

Figure 9(a) shows the 2D geometry of our encapsulated transducer (used in experiments) with detailed dimensions of the plates, silicone spacer, inner argon and outer fluid media. A proper mesh strategy has been deployed for better capture of acoustic wave. At least 12 or more elements

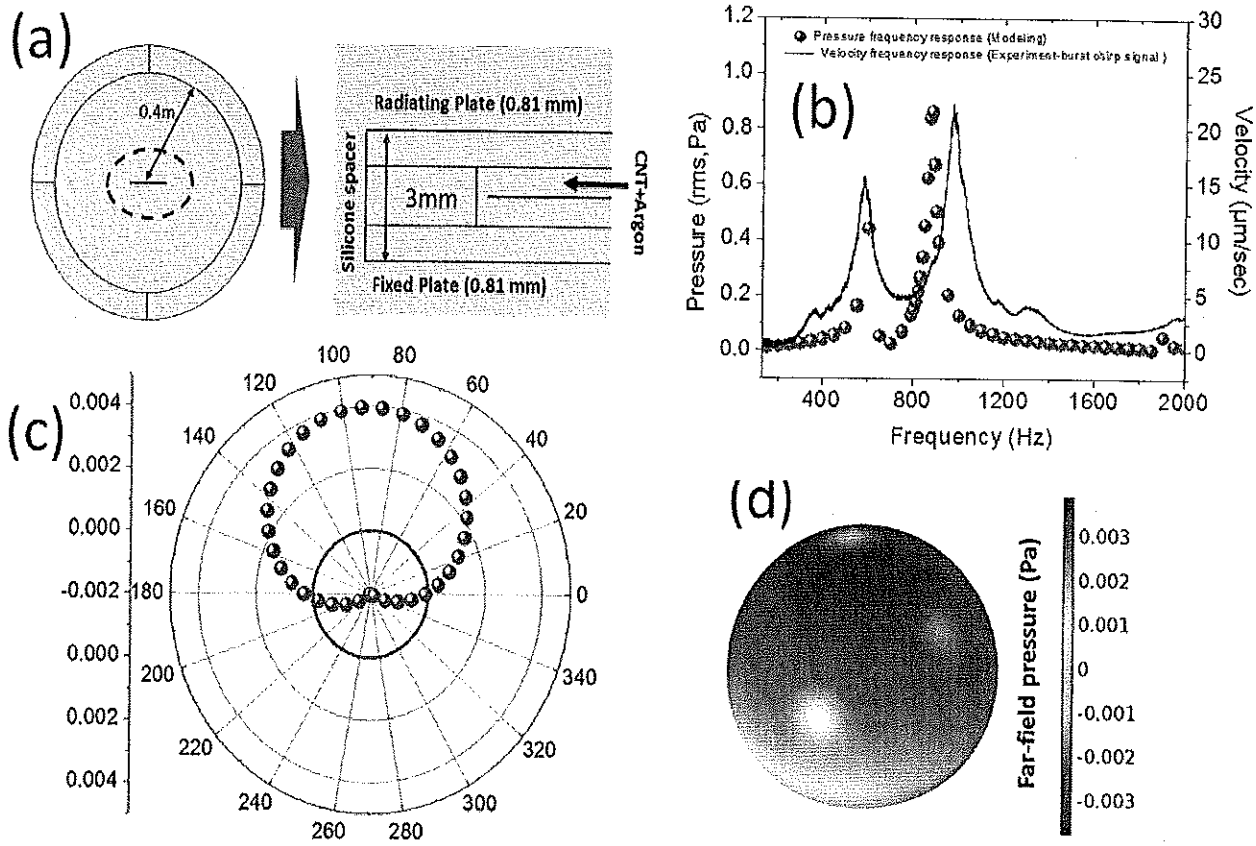

Figure 9: (a) Dimensions and computational domain for CNT-TA projector, (b) Frequency response (FR) of the device in air (2nd axis shows FR of experimentally measured velocity), (c) far-field pressure distribution of device in yz -plane (red circle represent the reference pressure, (d) 3D sound pressure far-field.

per wavelength are being used for computing the acoustic pressure. A perfectly matched layer (PML) is being used to create the non-reflective boundary for outgoing sound waves (at r = 0.4m from the device) and a swept meshing is being deployed for better transparency of the input acoustic wave at the end of the domain. For modeling, we followed similar conditions as that in experiments i.e. the bottom plate is fixed and only the top plate of the transducer is allowed to radiate sound. Figure 9(b) shows the frequency response curve of acoustic pressure for an encapsulated TA device in air. From modeling, we observed two prominent peaks (computed at r=3cm above the device) at frequencies of ~600 and 890 Hz.

This trend is very similar to the experimentally obtained velocity profile (velocity and acoustic pressure are always proportional). In experiment, the peak frequencies obtained were ~ 580 and 970Hz. The differences in frequency from the model are possibly due to non-linear behavior of the silicone rubber sealing at the edges and the entrained gas (in our case argon). In both cases

(modeling and experiment) the 2nd peak (or 2nd mode) frequency was dominant. Figures 9 (c) and (d) show a polar plot (yz- plane) and a 3D contour of the spatially distributive far-field pressure and the directivity of our numerical setup.

Figure 10 (a) shows the 1st mode velocity of the top aluminum plate of our transducer along the x-axis at different power input. It can be estimated that with an increase of power input the velocity

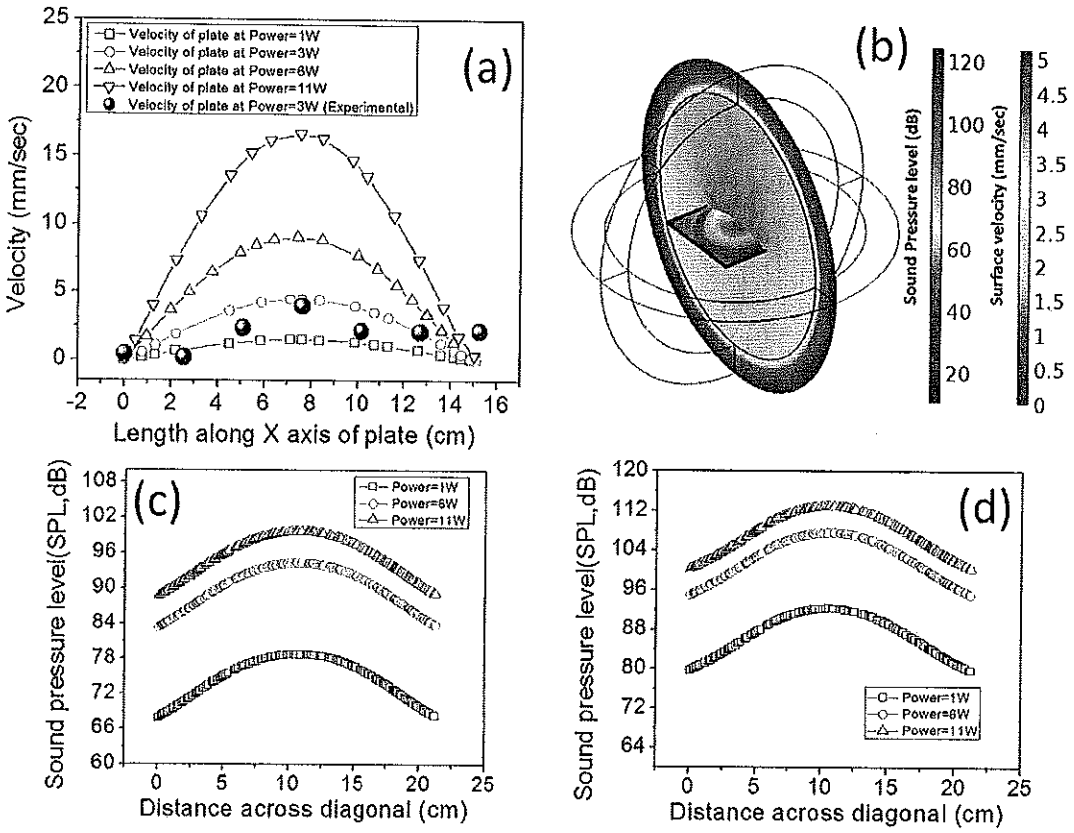

Figure 10: (a) Comparison of experimental and modeling results of the surface velocity of the TA projector (1st mode), (b) SPL and velocity representation of 2nd mode, (c) Sound pressure level for the 1st mode, (d) Sound pressure level for the 2st mode.

profile increases linearly. The numerically obtained solution is compared with a set of experimental results (obtained from Polytec-PSV500). The maximum velocity at the center of the plate obtained from modeling is 0.045 m/sec, as compared to the 0.04 m/s in experiment (at 3.0 W power input).

Figure 10 (b) shows the sliced view (yz-plane) of the model representing the spatial contour of pressure and structural velocity. Figure 10 (c) and (d) show a comparison of the sound pressure level (SPL) of the device (along the diagonal since the device is square in shape) for various power inputs and frequency = 600 Hz and 890 Hz, respectively. The difference we observed from our model is that with the same power input (~11W) the SPL differs by 12 dB. Our experiments as well as model demonstrates that the resonating encapsulated TA device performs well at 2nd peak frequency in air medium. We are moving forward with modeling the device (submerged) in a water medium. Figure 11(a) shows the frequency response of the device in water. The Figure 11(a) inset

shows the structural frequency response obtained experimentally. Both profiles are similar in the sense that, unlike in air, the 1st peak frequency is dominant. This behavior is observed in both the structural and acoustic pressure profiles from both experiment and modeling. The 1st and 2nd peak frequencies obtained from modeling are: 141 and 310 Hz. In experiments these were 167 and 315 Hz for particular depth conditions. The slight difference in modeling and experimental results is because of the existence of non-linear dynamic stiffness and damping at the edges in actual device. In water, the hydrostatic pressure could also affect the entrained gas behavior of the device. Figure 11 (b) shows the velocity profile trend of the upper plate at different power inputs, and a comparison with experimental data. It can be observed, that the experimental and modeling results are in close agreement. In Figure 11(c), we calculate the sound pressure with vertical distance at different power input and perform curve fit. From the graph it is evident that the vertical pressure is approximately proportional to the distance, which is supported by the theoretical pressure decay expression, *pressure ~1/r.* Detailed experimental underwater pressure tests are being compared with the outcomes of the integrated model. Figure 11(d) shows a comparison of experimental and modeling results for pressure output for different input powers. As can be observed, our model gives the linear trend with different power input which needs to be validated by the experimental results at different measured distances. This validation of our model with experimental results will provide the integrated numerical solution of the transducer which takes an input of thermal power and gives pressure in the outside fluid media. Figure 11 (e) shows the spatial thermal distribution

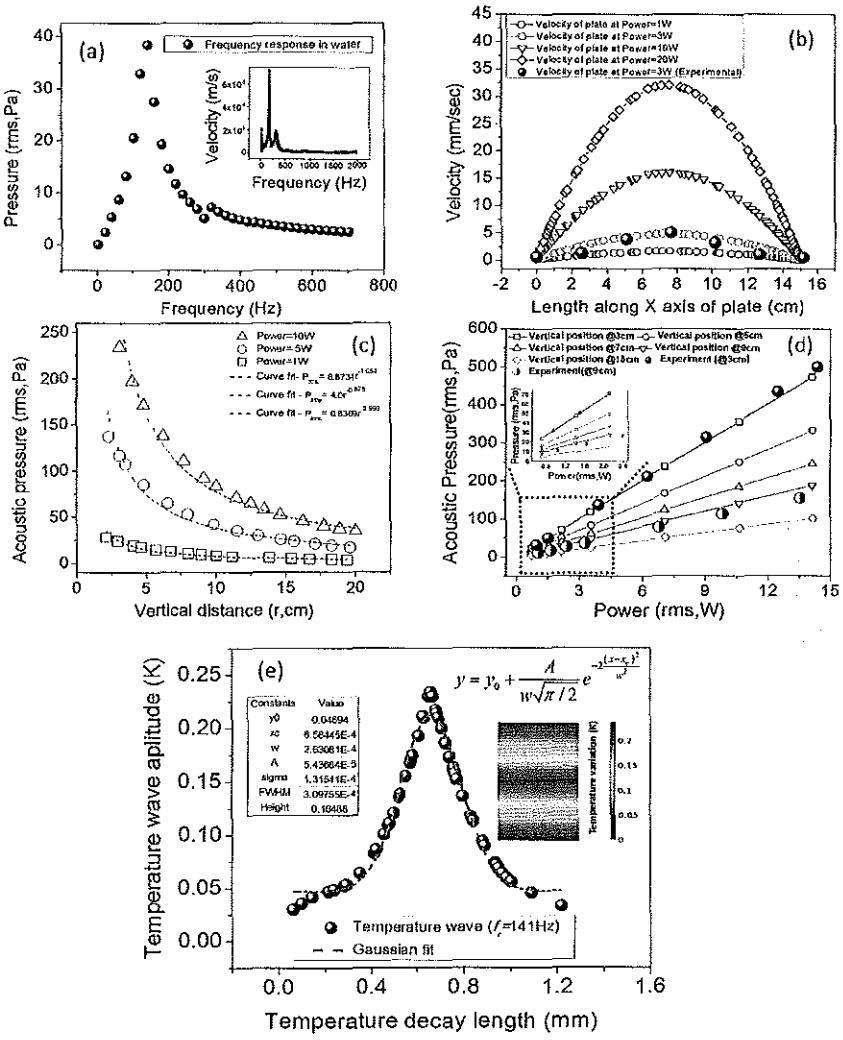

Figure 11: (a) Frequency response of the system obtained by numerical experiments in water medium, (b) Comparison of experimental and modeling results of surface velocity of the TA projector, (c) Sound pressure variation with increase of vertical depth, (d) experimentally obtained pressure value is compared with modeling,(e) Spatial distribution of temperature variation amplitude across the TA domain.

at the device resonance, which can be seen to exhibit a Gaussian profile. To summarize, a multilayer numerical solution is being developed for TA devices which predicts the acoustic pressure field with only an electrical input signal. Once the complete model has been assembled (electrical to thermal, thermal to pressure wave, pressure wave to acoustics) and validated, we will utilize the model to optimize new transducers. The optimized devices will be fabricated and tested in the large tank setup. We believe this complete model along with an optimized device will provide the low-frequency, high intensity, and high-efficiency TA projector from this program.

IMPACT/APPLICATIONS

- Integration of low frequency high power TA projectors on sea vehicles. This can help in SONAR application and oceanography
- Effective mean for underwater communication
- TA technology could be effectively used for sound therapy
- Underground oil recovery

References:

[1] Aliev AE, Gartstein YN, Baughman RH. Increasing the efficiency of thermoacoustic carbon nanotube sound projectors. Nanotechnology. 2013;24:235501.
[2] Arnold H, Crandall I. The thermophone as a precision source of sound. Physical review. 1917;10:22.
[3] Lim CW, Tong L, Li Y. Theory of suspended carbon nanotube thinfilm as a thermal-acoustic source. Journal of Sound and Vibration. 2013;332:5451-61.
[4] Xiao L, Chen Z, Feng C, Liu L, Bai Z-Q, Wang Y, et al. Flexible, stretchable, transparent carbon nanotube thin film loudspeakers. Nano letters. 2008;8:4539-45.
[5] Tian H, Xie D, Yang Y, Ren T-L, Wang Y-F, Zhou C-J, et al. Transparent, flexible, ultrathin sound source devices using indium tin oxide films. Applied Physics Letters. 2011;99:043503.
[6] Hu H, Zhu T, Xu J. Model for thermoacoustic emission from solids. Applied Physics Letters. 2010;96:214101.